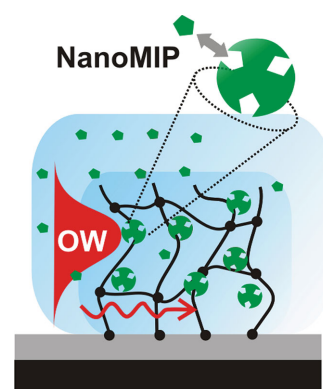


Molecularly Imprinted Polymer Waveguides for Direct Optical Detection of Low-Molecular-Weight Analytes

Nityanand Sharma, Christian Petri, Ulrich Jonas, Monika Bach, Günter Tovar, Kateřina Mrkvová, Milan Vala, Jiří Homola, Wolfgang Knoll, Jakub Dostálek*

New composite layer architecture of 3D hydrogel polymer network that is loaded with molecularly imprinted polymer nanoparticles (nanoMIP) is reported for direct optical detection of low-molecular-weight compounds. This composite layer is attached to the metallic surface of a surface plasmon resonance (SPR) sensor in order to simultaneously serve as an optical waveguide and large capacity binding-matrix for imprinted target analyte. Optical waveguide spectroscopy (OWS) is used as a label-free readout method allowing direct measurement of refractive index changes that are associated with molecular binding events inside the matrix. This approach is implemented by using a photocrosslinkable poly(*N*-isopropylacrylamide)-based hydrogel and poly[(ethylene glycol dimethylacrylate)-(methacrylic acid)] nanoparticles that are imprinted with *L*-Boc-phenylalanine-anilide (*L*-BFA, molecular weight 353 g mol⁻¹). Titration experiments with the specific target and other structurally similar reference compounds show good specificity and limit of detection for target *L*-BFA as low as 2×10^{-6} M.



N. Sharma, Prof. W. Knoll, Dr. J. Dostálek
Biosensor Technologies, AIT - Austrian Institute of Technology
GmbH, Muthgasse 11, Vienna 1190, Austria
E-mail: jakub.dostalek@ait.ac.at
N. Sharma, Prof. W. Knoll
Nanyang Technological University, Centre for Biomimetic
Sensor Science, Singapore 637553
C. Petri, Prof. U. Jonas
Macromolecular Chemistry, University of Siegen, Department
Chemistry-Biology, Adolf-Reichwein-Strasse 2, Siegen 57076,
Germany
Prof. U. Jonas
Foundation for Research and Technology Hellas (FORTH), Bio-
Organic Materials Chemistry Laboratory (BOMCLab), P.O. Box
1527, 71110 Heraklion, Crete, Greece

Dr. M. Bach, Prof. G. Tovar
Institute of Interfacial Process Engineering and Plasma
Technology IGVP, University of Stuttgart,
Nobelstraße 12, 70569 Stuttgart, Germany
Dr. M. Bach, Prof. G. Tovar
Fraunhofer-Institute for Interfacial Engineering and
Biotechnology IGB, Nobelstraße 12,
70569 Stuttgart, Germany
K. Mrkvová, M. Vala, Prof. J. Homola
Institute of Photonics and Electronics, Academy of Sciences
of the Czech Republic, Chaberská 57, 182 51
Prague, Czech Republic

1. Introduction

Numerous label-free optical sensor platforms were combined with molecularly imprinted polymers (MIP)^[1] for detection of chemical and biological analytes including those utilizing surface plasmon resonance (SPR),^[2,3] dielectric optical waveguides,^[4,5] reflection interference spectroscopy (RIFS),^[6,7] and diffractive structures.^[8–10] These optical sensors rely on the measurement of refractive index variations that are associated with a capture of target molecules by MIP on the sensor surface. With respect to established antibody recognition elements, the biomimetic MIP materials offer the advantage of superior stability and potentially lower cost. MIPs have been most often synthesized on the sensor surface in situ in the form of bulk polymer films by using thermal or photo-initiated polymerization in the presence of template molecules.^[11,12] However, this approach provides only limited density of accessible binding sites in close proximity to the outer surface of the MIP layer, which impedes the sensor sensitivity. In order to provide a more open structure, which can carry higher amounts of binding sites that are available for capture of diffusing target analyte, there were investigated MIP films, which were structured by using sacrificial colloidal crystals^[9,13] and optical lithography^[12] or formed by imprinting of loosely crosslinked hydrogels.^[14] These systems were reported to be capable of direct detection of small molecular analytes at typically μM – mM concentrations;^[3] however, several works reported the limit of detection at as low as pM concentrations.^[9,15]

Besides MIP layers, well-controlled synthesis of molecularly imprinted polymer micro- and nanoparticles (nanoMIP) was carried out by using precipitation, emulsion, or miniemulsion polymerization with a template dispersed in solution^[16] or attached to particle or bead carriers.^[17] NanoMIPs represent versatile materials that can be further processed and, e.g., their affinity purification allowed selecting nanoMIP fractions with dissociation affinity constants K_d as good as 10^{-8} – 10^{-9}M that makes them competing with regularly used antibodies.^[17,18] In optical sensor applications, nanoMIP monolayers were attached to the sensor surface by means of physisorption,^[19] affinity reactions,^[20] or covalent binding^[7] for the capture of target analyte.

The present work reports on a new material that holds potential to improve the sensitivity of MIP optical sensors. It is based on a composite film architecture comprising a hydrogel polymer network that is loaded with nanoMIPs. Such 3D structure can accommodate increased amounts of nanoMIPs compared to a 2D monolayer systems and it exhibits an open structure through which target molecules can rapidly diffuse to the imprinted binding pockets. Moreover, swollen hydrogel nanoMIP composite film can simultaneously serve as a waveguide,

which confines probing optical field in the region where specific molecular binding events occur.^[21,22]

2. Results and Discussion

As illustrated in Figure 1, composite polymer films were prepared by deposition from an ethanol solution with dispersed imprinted (nanoMIP) or control non-imprinted (nanoNIP) poly[(ethylene glycol dimethylacrylate)-(methacrylic acid)] nanoparticles (diameter $D \approx 190\text{ nm}$) that were mixed with a photo-crosslinkable poly(*N*-isopropylacrylamide) (pNIPAAm)-based hydrogel. After the solution was spun over the sensor surface, the layer was dried and crosslinked by irradiation with UV light ($\lambda = 365\text{ nm}$). The density of nanoparticles embedded in the film was controlled by the concentration of nanoMIP or nanoNIP (c_{NP}) and photo-crosslinkable pNIPAAm polymer (c_{pp}) in ethanol.

The cross-section of dry composite layers with varied nanoMIP density was observed by scanning electron microscopy (SEM). The obtained results presented in Figure 2a reveal that the amount of loaded nanoparticles increases with their concentration in solution (c_{NP} varied between 3 and 6 wt%) that was blended with pNIPAAm polymer at a fixed concentration ($c_{\text{pp}} = 1\text{ wt\%}$) and spun on the sensor surface. Thickness of the dry composite films $d_{\text{h-dry}}$ is increasing with polymer nanoparticle concentration c_{NP} and its morphology is changing. For high polymer nanoparticle concentrations c_{NP} , the interstitial volume between the nanoparticles is mostly void and pNIPAAm hydrogel is present only at contact areas between the polymer nanoparticles. For small polymer nanoparticle concentration c_{NP} , the volume of the film is mostly occupied by pNIPAAm hydrogel with sparsely distributed nanoparticles inside. Figure 2b shows that the morphologies of composite films loaded with same amounts of nanoMIP and nanoNIP are similar when using an identical protocol ($c_{\text{NP}} = 6\text{ wt\%}$ and $c_{\text{pp}} = 1\text{ wt\%}$).

The characteristics of composite films before and after their swelling in a working buffer (mixture of $80 \times 10^{-3}\text{ M}$ phosphate buffer and methanol at 1:1 ratio, pH 7) were observed by optical waveguide spectroscopy (OWS) that was implemented as shown in Figure 3a. In this optical setup, composite polymer film attached to the gold surface served as a waveguide, which confines light propagation by the highly reflective metallic surface and by total internal reflection at the interface between the composite film and liquid medium. Such films support multiple guided optical waves (OW - marked further as $\text{TM}_{1,2}$ and $\text{TE}_{0,1}$) that can be coupled with far field optical waves by using the Kretschmann configuration of the attenuated total reflection (ATR) method. The spectrum of guided waves was measured by using a laser beam with the



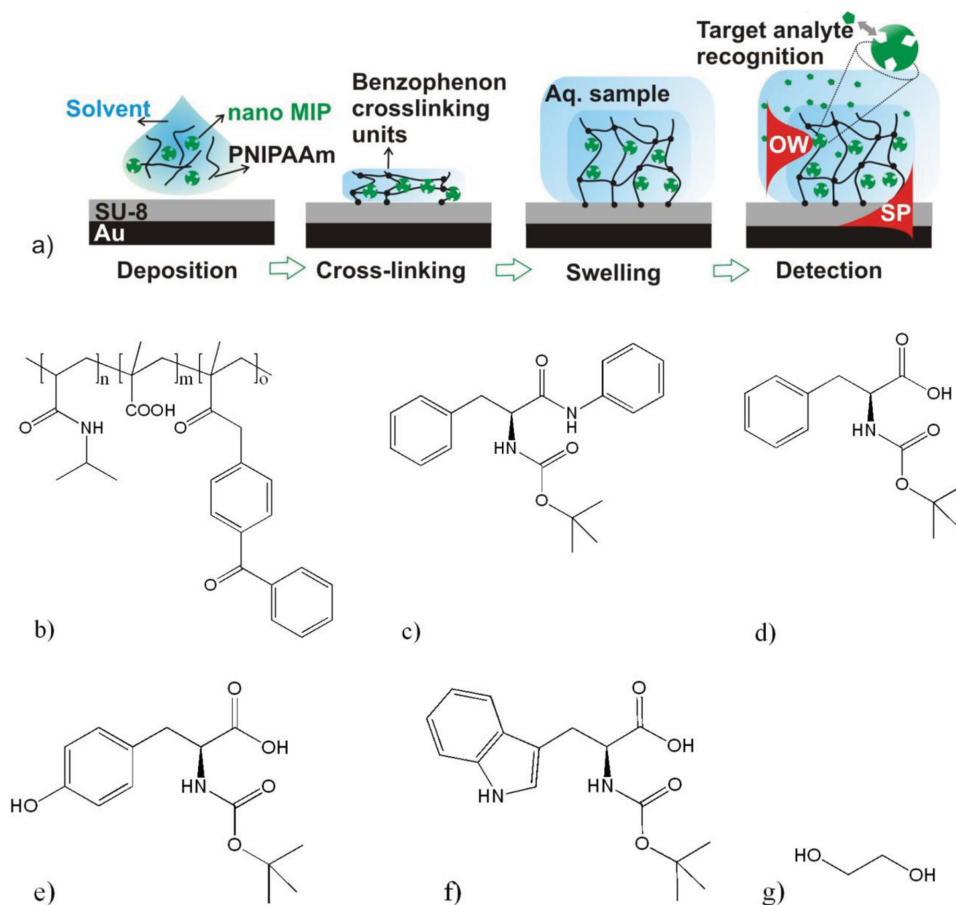


Figure 1. a) Preparation of composite layer with embedded nanoMIPs and chemical structure of used materials, b) poly(*N*-isopropylacrylamide-co-methacrylic acid-co-4-methacryloyloxy benzophenone) (pNIPAAm), c) *L*-Boc-phenylalanine-anilide (L-BFA), d) *L*-Boc-phenylalanine (L-BPA), e) *L*-Boc-tyrosine (L-BTS), f) *L*-Boc-tryptophan (L-BTP), g) ethylene glycol (EG).

wavelength of $\lambda = 632.8$ nm that was launched into a high refractive index prism with optically matched glass substrate carrying a stack of layers consisting of 47 nm gold, a thin SU-8 linker layer, and the composite film. The angle of incidence θ of the light beam hitting the surface was varied by using a rotation stage and the reflected beam intensity was detected by using a photodiode. In order to excite optical modes with transverse electric (TE) or transverse magnetic (TM) polarization, a rotational polarizer was used.

Figure 4a–d shows that the resonant excitation of guided waves in the composite polymer film is manifested as series of dips in the TM and TE angular reflectivity spectrum $R(\theta)$. As described further, fitting of these curves by a Fresnel reflectivity-based model was used for the determining of (complex) refractive index n_h of prepared layers as well as of their thicknesses in swollen d_h or dry $d_{h\text{-dry}}$ states. The real part of the refractive index $\text{Re}\{n_h\}$ relates to the density of the film and allowed us determining the total polymer volume fraction of the film f . Let us note that the polymer volume fraction is inversely proportional to the swelling ratio $f = 1/SR$, which

is defined as the ratio of thicknesses in the swollen and dry states $SR = d_h/d_{h\text{-dry}}$. Imaginary part of the refractive index $\text{Im}\{n_h\}$ reflects the damping of OW modes due to the scattering at nanoparticles embedded in the waveguide. In general, $\text{Re}\{n_h\}$ can be obtained by fitting the angular position of the resonance (angle θ_r at which the minimum of reflectivity dip occurs) and $\text{Im}\{n_h\}$ can be determined from the angular width of the resonance $\delta\theta_r$. Example of measured and fitted reflectivity curves in Figure 4 shows that studied films supported at least two OW modes in TE and TM polarizations. The simultaneous analysis of multiple OW modes allowed for independent determining of thicknesses d_h and $d_{h\text{-dry}}$ as well as respective refractive index n_h . As can be seen in Figure 4b, the resonant coupling to SP mode occurs at significantly lower angle than model based on fitting OW modes suggests. The reason is that the average refractive index of the composite slice, which is probed by SPs (distance up to about 100 nm from the gold surface) comprises only a small portion of nanoparticles with the diameter $D \approx 190$ nm and thus obtained n_h is different from that determined by the analysis of OWs (that is averaged across the

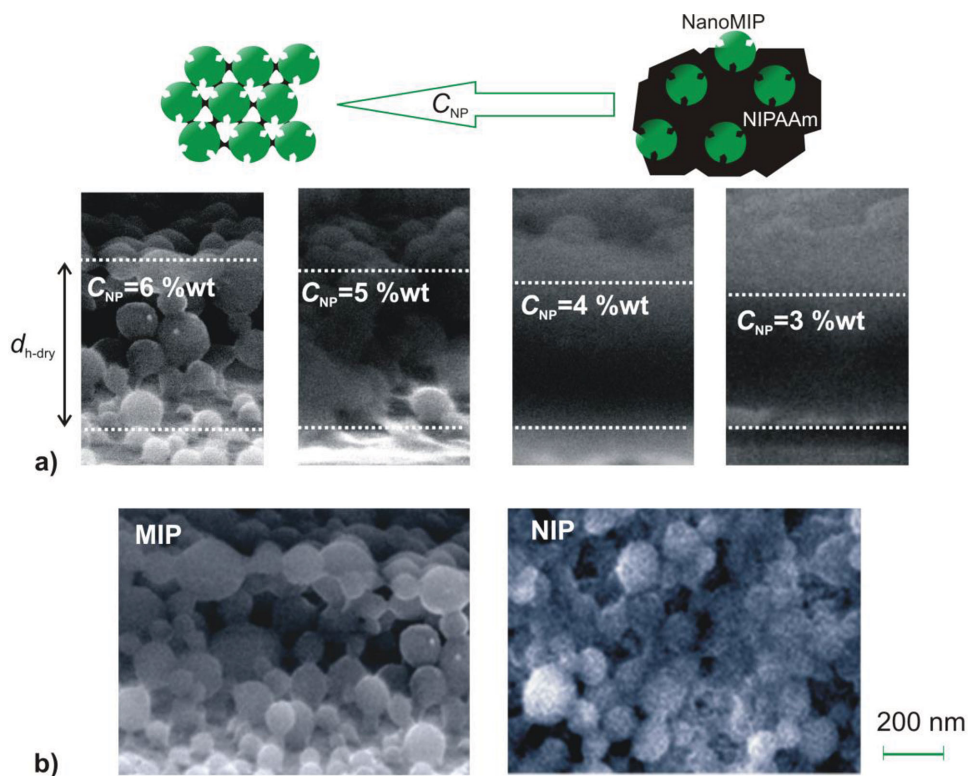


Figure 2. SEM cross-section images of dry a) nanoMIP composite films prepared from a solution with $c_{pp} = 1$ wt% and $c_{NP} = 3-6$ wt% and b) comparison of nanoMIP (left) and nanoNIP (right) structures.

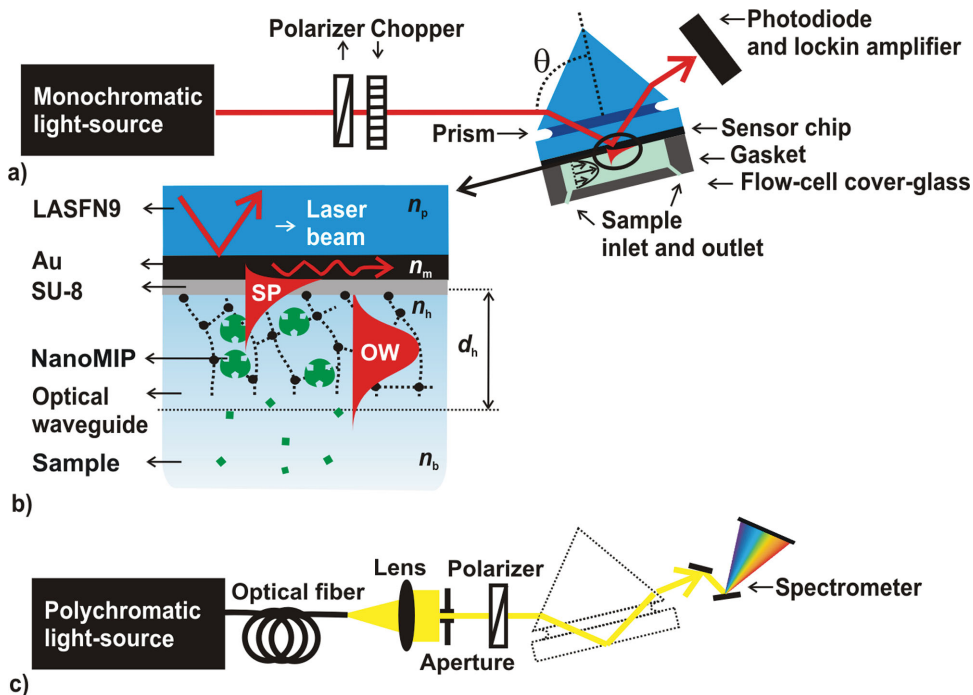


Figure 3. Schematic of sensor surface architecture and optical setup used for optical waveguide spectroscopy utilizing a surface plasmon resonance spectrometer with: a) angular and c) wavelength interrogation. b) Detail of the sensor surface architecture with the polymer composite waveguide.

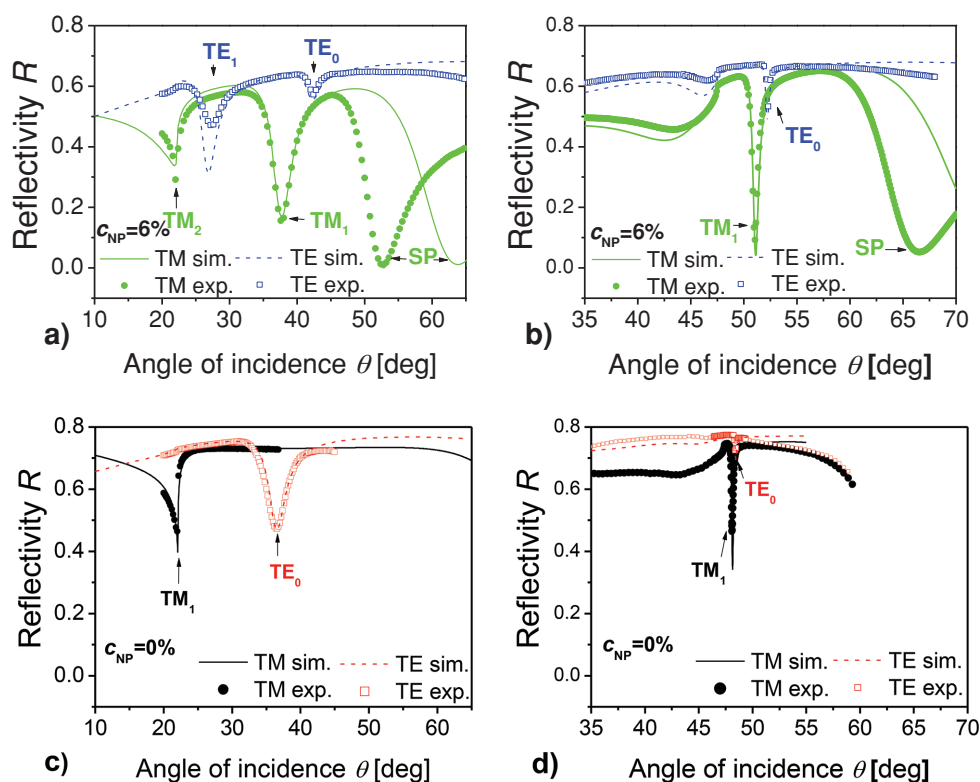


Figure 4. Angular reflectivity spectra for dry (left a and c) and swollen (right b and d) layers prepared from a solution with concentration of nanoMIP $c_{NP} = 6$ wt% and pNIPAAm $c_{pp} = 1$ wt% (top a and b) compared to that prepared from a solution with $c_{NP} = 0$ wt% and $c_{pp} = 3$ wt% (bottom c and d). Measured and fitted curves for transverse magnetic (TM) and transverse electric (TE) polarization are shown as indicated in graphs.

whole, around micrometer thick, composite film). Therefore, only OW resonances $TE_{0,1}$ and $TM_{1,2}$ were fitted and the SP resonance was omitted in further analysis.

The thickness of dry composite film that was prepared from the solution with dissolved pNIPAAm at the concentration of $c_{pp} = 1$ wt% and polymer nanoparticles with the concentration $c_{NP} = 6$ wt% was fitted as $d_{h-dry} = 587$ nm (Figure 4a), which is in accordance with SEM observations presented in Figure 2. In working buffer, pNIPAAm in this composite layer swells, which leads to an increase in its thickness to $d_h = 814$ nm and corresponds to the swelling ratio of $SR = 1.39$ (see Figure 4b). This value is much smaller than $SR = 5.42$ obtained for a film, which was prepared in identical way from only pNIPAAm polymer ($c_{pp} = 3$ wt% and $c_{NP} = 0$ wt%), see Figure 4c,d. The reason

for the hindered expansion of the composite films is that the embedded nanoMIP (or nanoNIP) nanoparticles swell much weaker compared to pNIPAAm-based hydrogel. In addition, they react with the benzophenon groups and thus can serve as an additional “supercrosslinking” nodes as was shown by previous studies with other nanoparticles.^[23] As the overview in Table 1 presents, the imaginary part of fitted refractive index $\text{Im}\{n_h\}$ is order of magnitude higher for dry composite film than for a dry film composed of only pNIPAAm-based polymer. However, $\text{Im}\{n_h\}$ of the composite film with nanoMIP drops after the swelling in a working buffer and its value reaches $\text{Im}\{n_h\}$ for the film without nanoMIP. The reason is that the filling of voids in the composite structure with working buffer decreases the refractive index difference

Table 1. Comparison of fitted parameters for composite structures with and without nanoMIP.

c_{NP}/c_{pp} [wt%]	d_h or d_{h-dry} [nm]	$\text{Re}\{n_h\}$	$\text{Im}\{n_h\}$	SR	f
0/3 (Dry)	206	1.480	$<10^{-3}$	5.42	1.00
0/3 (Swollen)	1116	1.361	$<10^{-3}$		0.19
6/1 (Dry)	587	1.335	0.014	1.39	0.73
6/1 (Swollen)	814	1.420	0.002		0.59

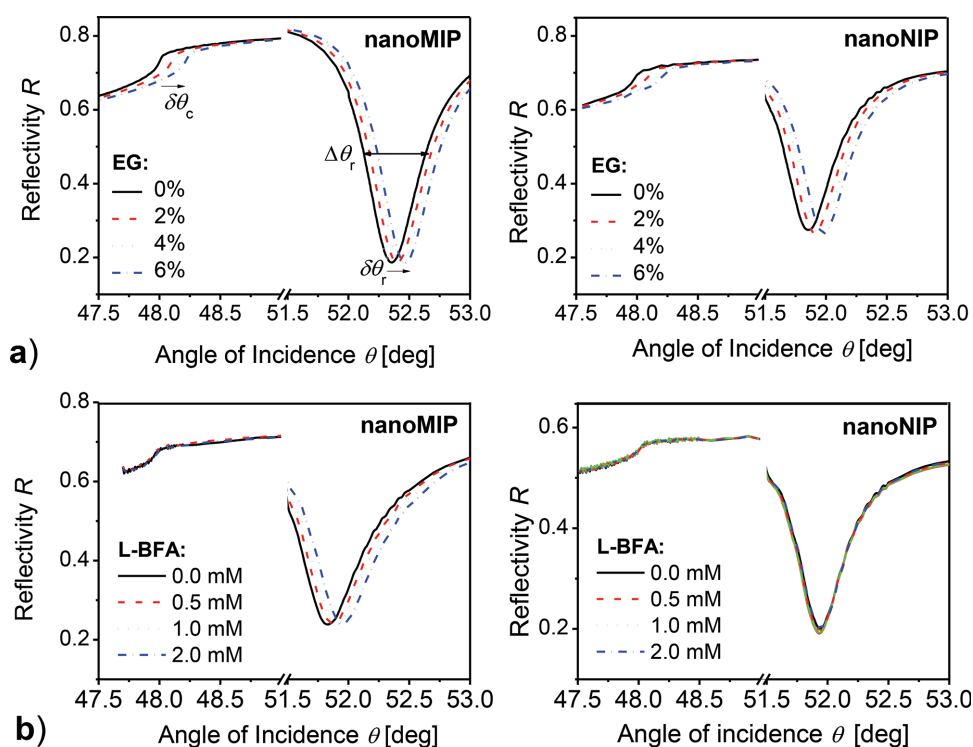


Figure 5. Measured angular reflectivity spectra for nanoMIP (left) and nanoNIP (right) composite film ($c_{\text{NP}} = 6$ wt% and $c_{\text{pp}} = 1$ wt%) that were brought in contact with a buffer spiked with a) reference ethylene glycol and b) target analyte L-BFA.

between nanoMIP ($n_p = 1.48$) and surrounding environment ($n_b = 1$ for air and ≈ 1.325 for working buffer), which reduces of the scattering losses of the waveguide.

For dry composite films, the total polymer volume fraction f (including both the nanoMIP and pNIPAAm polymers) is decreasing with the nanoMIP concentration c_{NP} due to the occurrence of void interstitial space (see Figure 2). However, an opposite behavior is observed when the films are swollen in working buffer due to the restricted swelling. For example, swollen layer composed of only a pNIPAAm hydrogel (prepared with $c_{\text{NP}} = 0$ wt% and $c_{\text{pp}} = 3$ wt%) exhibited the polymer volume fraction of $f = 19\%$. When nanoMIP were loaded into the pNIPAAm network (composite layer prepared from a solution with $c_{\text{NP}} = 6$ wt% and $c_{\text{pp}} = 1$ wt%), a significantly higher total polymer volume fraction of $f = 59\%$ was determined. Let us note that SEM observations in Figure 2b suggest that the majority of polymer volume in such composite film is occupied by nanoMIPs and the polymer volume fraction measured by OWS approaches the value corresponding to maximum space filling for ordered colloidal crystals ($f = 74\%$).^[24] Assuming that the volume of spherical nanoMIPs is $\pi D^3/6$, the average number of nanoparticles per volume can be estimated as $6(f/\pi D^3)^{-1}$, which yields $\approx 4 \times 10^2 \mu\text{m}^{-3}$ for the composite layer prepared from a solution with $c_{\text{NP}} = 6$ wt% and $c_{\text{pp}} = 1$ wt%. Such composite films with high density of nanoMIP or nanoNIP were stable upon repeated swelling and drying cycles and we observed no

changes in their binding characteristics when stored at ambient environment for over 4 months.

The prepared composite films exhibit voids (with the relative volume $[1-f]$) through which small molecules can rapidly diffuse. In order to prove this, refractive index changes induced by ethylene glycol (EG, molecular weight 67 g mol^{-1}) diffusing through the composite film were observed by OWS. Figure 5a shows measured angular reflectivity spectra with TM_1 resonance on the sensor surface carrying composite film loaded with nanoMIP (left) and nanoNIP (right). Both layers were prepared by identical protocol from a solution with $c_{\text{NP}} = 6$ wt% and $c_{\text{pp}} = 1\%$ and they were successively brought in contact with working buffer spiked with increasing concentration of EG. An increase in the refractive index of working buffer δn_b due to the spiking with EG is manifested as a shift in the critical angle θ_c . In addition, as EG molecules diffuse from a solution into composite film they change its (effective) refractive index n_h which leads to the shift in the resonant coupling angle θ_r . Shifts of $\delta\theta_r = 0\text{--}0.12^\circ$ were observed upon successive flow of working buffer spiked with EG at concentrations between 0 and 6 vol% (which corresponds to the buffer refractive indices of $n_b = 1.325\text{--}1.331$ as determined from changes in θ_c). The TM_1 resonant angle shifts linearly with the refractive index sensitivity (slope) of $S = \delta\theta_r/\delta n_b = 24.5^\circ$ per refractive index unit (RIU) for both nanoMIP and nanoNIP composite films. This value translates to the figure of merit

in refractometric measurements of $FOM = 52$ ($FOM = S/\theta_r$, – defined as the ratio of refractive index sensitivity S and the resonance full width at half minimum θ_r) taking into account the width of TM_1 resonant dip of $\theta_r = 0.47^\circ$. Such FOM is more than twofold better than that for regular SPR at the same wavelength ($FOM = 20.8 \text{ RIU}^{-1}$) but it is about 15 times lower than that observed for similar pNI-PAAm hydrogel waveguide that was modified with small biomolecules ($FOM = 810 \text{ RIU}^{-1}$).^[21] The reason is that the loading of nanoMIPs or nanoNIPs into the waveguide leads to the increased imaginary part of the refractive index $\text{Im}\{n_h\}$ (due to the scattering of the guided mode on nanoparticles) and subsequently to higher resonance width θ_r (increased by a factor of about five). In addition, the presence of nanoMIP increases the total polymer volume fraction f and thus smaller volume accessible for diffusing of analyte (sensitivity S and accessible volume proportional to $(1 - f)$ is decreased by a factor of 2–3 with respect to the structure without nanoMIP).^[21]

In order to characterize the specificity and binding capacity of imprinted cavities on the sensor surface, measuring (nanoMIP) and reference (nanoNIP) composite films were probed by TM_1 resonance upon a flow of series of samples spiked with L-BFA at concentrations between 0 and $2 \times 10^{-3} \text{ M}$. As respective angular reflectivity curves in Figure 5b show, the flow of L-BFA is accompanied with a shift of the resonant angle $\delta\theta_r$ due to the binding-induced refractive index changes, which are about nine times higher for the nanoMIP composite film than for the reference surface with nanoNIPs. Such results indicate that the interaction of L-BFA with imprinted cavities leads to efficient accumulation of analyte in the film and that the non-specific interaction of L-BFA with used polymers is much weaker. The accumulation of target analyte in composite films was estimated from refractive index changes determined from measured shifts of the resonance coupling angle $\delta\theta_r$ and critical angle $\delta\theta_c$ (we assumed that the change in the thickness d_h due to the swelling of nanoMIP or nanoNIP that is associated with the affinity interaction with target L-BFA molecules was negligible and that the composite films change only their refractive index n_h). This analysis shows that the presence of target analyte at the $1 \times 10^{-3} \text{ M}$ concentration increases refractive index in the liquid sample by $\delta n_b \approx 7 \times 10^{-5} \text{ RIU}$ and leads to the increase of refractive index of nanoMIPs composite layer of $\delta n_h \approx 3 \times 10^{-3} \text{ RIU}$. Assuming the refractive index increases linearly with the concentration of L-BFA and the composite film has slightly higher RI (so that the same amount of L-BFA will cause about 10% less RI change δn_h than δn_b), these data indicate that the concentration of L-BFA accumulated in the nanoMIP composite film is increased by a factor of ≈ 46 with respect to that in the bulk sample solution. Much weaker accumulation was observed for the control nanoNIP films (measured value

of $\delta n_h \approx 2.7 \times 10^{-4} \text{ RIU}$ corresponds to the factor of ≈ 4), which indicates successful imprinting. It should be noted that nanoMIP nanoparticles exhibited surface area that was larger only by a factor of 1.23 with respect to that of nanoNIP as determined by gas adsorption experiment.^[25] Therefore, the 10-times stronger accumulation of L-BFA in the nanoMIP composite film compared to that on the reference nano-NIP surface cannot be explained by unspecific interaction between the analyte and used polymers. Comparing the concentration of preconcentrated analyte inside the nanoMIP layer with the density of imprinted nanoparticles, the number of binding pockets per nanoparticle can be estimated as 10^2 – 10^3 , which agrees with previous studies.^[25]

For more detailed studies of affinity interaction of specific L-BFA and other structurally similar control analytes with the nanoMIP and nanoNIP composite films, wavelength spectroscopy of guided waves was employed. As Figure 3c shows, a source of collimated polychromatic light beam was coupled to a glass prism and made incident at a fixed angle of incidence on the optically matched sensor chip with nanoMIP or nanoNIP layers (let us note that identical waveguides as in previous angular modulation studies were used). The angle of incidence θ was adjusted in such a way that the resonant excitation of TM_1 optical waveguide mode occurred in the vicinity to the wavelength of $\lambda = 632.8 \text{ nm}$ (the same as used in the previous angular modulation study). This TM_1 resonance is manifested as a narrow dip in the wavelength spectrum of reflected beam intensity, which was measured by a spectrometer. The refractive index-induced variations in the resonant wavelength $\delta\lambda_r$ were fitted in real time from measured wavelength spectra. The standard deviation of the sensor signal was $\sigma_\lambda = 3 \times 10^{-3} \text{ nm}$ and the bulk refractive index sensitivity was about $S = \delta\lambda_r/\delta n_b = 5 \times 10^3 \text{ nm/RIU}$, which translates to the refractive index resolution of $\sigma_\lambda/S \approx 6 \times 10^{-7} \text{ RIU}$ (this resolution was more than order of magnitude better than that for previously used setup utilizing angular spectroscopy of guided waves). Prior to the measurement of resonance wavelength changes $\delta\lambda_r$ due to the affinity interaction of studied analytes, the sensor was calibrated in order to take into account small chip-to-chip variations and inaccuracies in the optical alignment. First, the resonant wavelength change $\delta\lambda_{r0}$ due to the flow of a working buffer with 0.5 vol% of EG was measured and the sensor output was determined as the ratio $\delta\lambda_r/\delta\lambda_{r0}$.

As seen in Figure 6a, a baseline in the sensor output was firstly established upon the flow of a working buffer. Afterwards, a series of samples spiked with L-BFA was sequentially injected to the sensor and let interact with the composite film for 10 min followed by rinsing for 10 min. Measured data show that the L-BFA binding results in a gradual shift in the sensor output $\lambda_r/\delta\lambda_{r0}$,

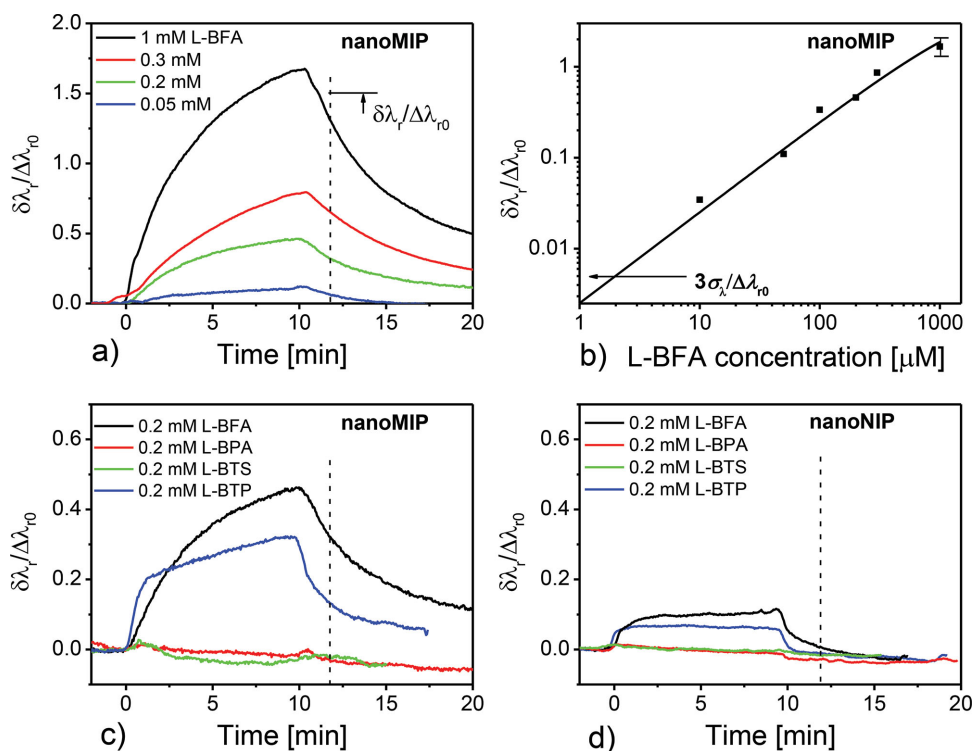


Figure 6. a) Kinetics of affinity binding of target L-BFA to nanoMIP waveguide at concentrations indicated in the inset and b) corresponding calibration curve with the error bar showing standard deviation of the response measured in triplicate on different waveguide chips. Comparison of binding kinetics of target analyte L-BFA and structurally similar reference analytes L-BTP, L-BPA, and L-BTS on c) measuring nanoMIP and d) control nanoNIP waveguides.

which saturates at levels that increases with the L-BFA concentration. Further, the sensor response was defined as the difference in the sensor output $\delta\lambda_r/\delta\lambda_{r0}$ before the injection of a sample and after the 2 min rinsing (indicated as a dashed line in Figure 6a). The 2 min rinsing time was sufficiently long to replace the sample from the flow-cell by working buffer and thus eliminate the effect of the sensor output change due to the bulk refractive index change δn_b . Obtained calibration curve presented in Figure 6b reveals that the response increases with the L-BFA concentration. From these data, limit of detection (LOD) of 2×10^{-6} M was determined as $3\sigma_\lambda/(d\lambda_r/dc)$.

The specificity of the developed MIP OWS sensor for the detection of L-BFA was tested by comparing the response of nanoMIP and nanoNIP waveguides to target L-BFA and other structurally similar reference analytes summarized in Figure 1c–f: L-Boc-Tryptophan (L-BTP), L-Boc-phenylalanine (L-BPA), and L-Boc-tyrosine (L-BTS). First, the obtained data show that the response $\delta\lambda_r/\delta\lambda_{r0}$ to target L-BFA analyte at concentration of 0.2×10^{-3} M was around 14 times higher for the nanoMIP waveguide (Figure 6c) than for the control nanoNIP (Figure 6d), which is consistent with previous angular modulation measurements presented in Figure 5b. The interaction of structurally similar L-BTP dissolved at same concentration of 0.2×10^{-3} M

resulted in around twofold lower response on nanoMIP surface than the target analyte L-BFA. On the control nanoNIP waveguide, the response to L-BTP was below values that can be reproducibly measured. The other reference analytes L-BPA and L-BTS showed non-measurable response on both nanoMIP and nanoNIP surfaces. Let us note that for L-BFA and L-BTP, a rapid change in the kinetics is observed in Figures 6c and d after injecting the sample ($t = 0$) and working buffer ($t = 10$ min). It is probably caused by a bulk refractive index change, which was caused by a small variation in the amount of methanol (added due to the weaker solubility of these analytes). In general, the measured data on selectivity of L-BFA imprinted nanoMIP are in line with previous studies and reveal that using of pNIPAAm hydrogel as a “glue” in the composite layer provided accessibility to MIP binding pockets, did not altered their affinity with target L-BFA analyte, and allowed improving sensitivity compared to other platforms for direct optical detection of small molecules that utilize 2D MIP coatings. For instance, the achieved limit of detection is about 30 times better than that reported for an optical sensor utilizing reflectometric interference spectroscopy (RIFS) with identically prepared L-BFA-imprinted nanoparticles that were attached to the surface in form of 2D layer.^[7] This advancement can be attributed to the higher refractometric sensitivity of the

OWS readout format and large-binding capacity that is offered by the 3D composite film architecture.

3. Conclusion

A new MIP architecture and readout method that is attractive for direct optical detection of low-molecular-weight analytes is reported. It is based on molecularly imprinted polymer nanoparticles (nanoMIP) that are embedded in a photo-crosslinkable hydrogel in order to provide high density of easily accessible imprinted moieties. Such composite films efficiently accumulate target analyte (about 10-fold increased concentration was observed as compared to films with non-imprinted nanoparticles – nanoNIPs) and at the same time can act as an optical waveguide. The spectroscopy of guided waves supported by the composite nanoMIP film allowed for accurate readout of refractive index variations associated with the interaction of target analyte and MIP moieties. OWS can be performed using regular SPR optical setup and it enables direct label-free detection of a model low-molecular-weight analyte – L-BFA – with an LOD as small as 2×10^{-6} M. The presented approach is generic and the using of photo-crosslinkable hydrogel allows for lithography or inject printing preparation of MIPs patterns. For instance, sensor chips carrying arrays of measuring and reference pads with different MIP moieties can be prepared in a much more straightforward and simple way than in case of traditional surface synthesis of MIPs on planar films. We believe that such advancements will allow harnessing current progress in the field of synthesis of high affinity MIP nanostructures (plastic antibody) and open a new door to development of next generation of sensitive and robust MIP sensors capable of multi-analyte and reference-compensated measurements.

4. Experimental Section

4.1. Materials

L-Boc-phenylalanine-anilide (L-BFA) with the molecular weight of 353 g mol^{-1} and reference non-target analytes including ethylene glycol (EG) with 62.07 g mol^{-1} , L-Boc-phenylalanine (L-BPA) with 265.3 g mol^{-1} , L-Boc-Tryptophan (L-BTP) with 304.3 g mol^{-1} , and L-Boc-tyrosine (L-BTS) with 281.3 g mol^{-1} were obtained from Sigma-Aldrich. Methanol and ethanol of analysis grade was purchased from Merck Millipore. Sodium dihydrogen phosphate (NaH_2PO_4) was purchased from Sigma-Aldrich. Working buffer was prepared from $80 \times 10^{-3} \text{ M NaH}_2\text{PO}_4$ aqueous solution (with the pH adjusted to 7 by titrating NaOH) that was mixed with methanol at volumetric ratio of 1:1. After adding the methanol and spiking the working buffer with specific and reference analytes, all salts in the solution were dissolved. SU-8 2000 and its

thinner (SU-8 2000 thinner) was purchased from Micro Resist Technology GmbH, Germany.

4.2. Synthesis of Polymers

Molecularly imprinted polymer nanoparticles were synthesized by thermal initiated miniemulsion polymerization as reported previously.^[16,26] Two sets of poly[(ethylene glycol dimethylacrylate)–(methacrylic acid)] nanoparticles were prepared, one was imprinted with L-BFA template molecule (nanoMIP) and the second was not imprinted with the template molecule (nanoNIP). p-NIPAAm-based hydrogel (composed of N-isopropylacrylamide, methacrylic acid, and 4-methacryloyloxy benzophenone at a ratio of 94:5:1, respectively, as seen in Figure 1b) was synthesized as reported before.^[27]

4.3. Preparation of NanoMIP Composites

LSFN9 glass substrates were coated by vacuum thermal evaporation with 1.1 nm thick chromium and 47 nm thick gold layers. On the top of the gold surface, an SU-8 polymer film with a thickness of about 10 nm was spin-coated from $c = 4.8 \text{ vol}\%$ solution (dissolved by SU-8 thinner) at spin rate 6000 rpm in order to serve as a linker for the subsequent attachment of a composite film. After the spin-coating of SU8, substrates were dried in a vacuum oven at $50 \text{ }^\circ\text{C}$ for 2 h. For the preparation of composite layers, an ethanol solution with nanoparticles ($c_{\text{NP}} = 0\text{--}6 \text{ wt}\%$) and pNIPAAm polymer ($c_{\text{pp}} = 1 \text{ wt}\%$) were spin-coated at the spin rate 2000 rpm for 2 min. Prior to the spin-coating, the particle solution was sonicated (Elmasonic S10) for 30 min in order to reduce aggregation. Composite polymer layers were dried in a vacuum oven overnight at $50 \text{ }^\circ\text{C}$ and cross-linked by UV light ($\lambda = 365 \text{ nm}$) with the irradiation dose of 25 J cm^{-2} . Then, layers were extensively rinsed with ethanol in order to remove loosely bound polymer chains and polymer nanoparticles followed by drying in a stream of air.

4.4. Imaging of NanoMIP Composites

The observation of morphology of prepared layers was performed by using SEM (Carl Zeiss EVO, a low voltage of 5 kV was used). In order to image the cross-section of the prepared layers, a substrate was broken and an angular stage was used for SEM imaging of the exposed layer edge.

4.5. Optical Setups

Angular reflectivity spectra $R(\theta)$ were measured by SPR spectrometer with Kretschmann configuration that was described in our previous works.^[21] Briefly, monochromatic laser beam from a He-Ne laser ($\lambda = 632.8 \text{ nm}$) was coupled to a LASFN9 glass prism and reflected from the base of prism for an angle of incidence θ . A sensor chip was optically matched to the prism base by using index matching immersion oil. The excitation of SP and OW waves by the laser beam hitting the gold layer was observed from the angular reflectivity spectra $R(\theta)$ measured by using a photodiode detector and a rotation stage with resolution of

coupling angle $\theta = 0.005^\circ$. The kinetics of affinity binding reactions was observed by using another SPR spectrometer that utilized wavelength modulation of resonant coupling to guided waves.^[28] In this system, a polychromatic light from a super-continuum source (WhiteLase micro, Fianium, UK) was collimated and made incident on BK7 glass prism at a fixed angle θ . Reflected light was coupled into a spectrometer (S2000, Ocean Optics, USA) to perform spectral analysis and wavelength shifts in resonant dips occurring in the wavelength reflectivity spectrum $R(\lambda)$ were determined in time by a dedicated software SPR UP (developed at the Institute of Photonics and Electronics in Prague, Czech Republic). In both measurements with angular and wavelength modulation, identical composite layers were used. Against the sensor surface carrying composite waveguide with nanoMIP or nanoNIP, a flow cell was attached and analyzed samples prepared from a working buffer were pumped by using a peristaltic pump with a Tygon MHL tubing (IDEX Health & Science SA, Switzerland).

4.6. Optical Properties of the Composites

Thickness and refractive index of composite layers were determined by the fitting angular reflectivity spectra $R(\theta)$ measured by an optical setup with angular modulation of SPR. These spectra were analyzed by using a Fresnel reflectivity-based model implemented in Winspall software (developed at Max Planck Institute for Polymer Research in Mainz, Germany). This tool allows fitting of refractive indices and thicknesses of used stack of layers (in which we assumed that the birefringence is negligible) by least squares method. From the fitted refractive index of the composite film that is swollen n_h , the polymer volume fraction f in the swollen state was obtained from effective medium theory as:

$$f = \frac{\left(\operatorname{Re}\{n_h\}^2 - n_b^2\right)\left(\operatorname{Re}\{n_p\}^2 + 2n_b^2\right)}{\left(\operatorname{Re}\{n_h\}^2 + 2n_b^2\right)\left(\operatorname{Re}\{n_p\}^2 - n_b^2\right)} \quad (1)$$

where n_b is refractive index of the solvent (working buffer) and $n_p = 1.48$ is the refractive index of the used polymers. It should be noted that a “box” model was used as prepared composite films were assumed to be homogeneous perpendicular to the surface. Prior to fitting of n_h , d_h , and $d_{h\text{-dry}}$, parameters of other chromium, gold and SU-8 layers were determined on reference samples.

Acknowledgements: The authors gratefully acknowledge partial support from the Austrian Science Fund (FWF) through the ACTIPLAS project (P 244920-N20), the Praemium Academiae of the Academy of Sciences of the Czech Republic and by the Czech Science Foundation (P205/12/G118), by the Carl Zeiss Stiftung via funding the Projektthaus NanoBioMater, and the Austrian Federal Ministry for Transport, Innovation and Technology (GZ BMVIT-612.166/0001-III/11/2010) via the International Graduate School Bio-Nano-Tech, a joint Ph.D. program of the University of Natural Resources and Life Sciences Vienna (BOKU), the Austrian Institute of Technology (AIT), and Nanyang Technological University (NTU).

Received: May 15, 2014; Revised: August 7, 2014; Published online: ;
DOI: 10.1002/mcp.201400260

Keywords: label-free biosensors; hydrogels; molecularly imprinted polymers; nanoparticles; optical waveguides spectroscopy

- [1] O. Y. F. Henry, D. C. Cullen, S. A. Piletsky, *Anal. Bioanal. Chem.* **2005**, *382*, 947.
- [2] M. Lotierzo, O. Y. F. Henry, S. Piletsky, I. Tothill, D. Cullen, M. Kania, B. Hock, A. P. F. Turner, *Biosens. Bioelectron.* **2004**, *20*, 145.
- [3] R. B. Pernites, R. R. Ponnappati, R. C. Advincola, *Macromolecules* **2010**, *43*, 9724.
- [4] N. R. Walker, M. J. Linman, M. M. Timmers, S. L. Dean, C. M. Burkett, J. A. Lloyd, J. D. Keelor, B. M. Baughman, P. L. Edmiston, *Anal. Chim. Acta* **2007**, *593*, 82.
- [5] C. A. Barrios, S. Carrasco, M. Francesca, P. Yurrita, F. Navarro-Villoslada, M. C. Moreno-Bondi, *Sens. Actuators, B* **2012**, *161*, 607.
- [6] D. Nopper, O. Lammershop, G. Wulff, G. Gauglitz, *Anal. Bioanal. Chem.* **2003**, *377*, 608.
- [7] F. Kolarov, K. Niedergall, M. Bach, G. E. M. Tovar, G. Gauglitz, *Anal. Bioanal. Chem.* **2011**, *402*, 3245.
- [8] Y. Fuchs, O. Soppera, A. G. Mayes, K. Haupt, *Adv. Mater.* **2013**, *25*, 566.
- [9] J. H. Li, Z. Zhang, S. F. Xu, L. X. Chen, N. Zhou, H. Xiong, H. L. Peng, *J. Mater. Chem.* **2011**, *21*, 19267.
- [10] C. A. Barrios, C. Zhenhe, F. Navarro-Villoslada, D. Lopez-Romero, M. C. Moreno-Bondi, *Biosens. Bioelectron.* **2011**, *26*, 2801.
- [11] A. G. Mayes, M. J. Whitcombe, *Adv. Drug Delivery Rev.* **2005**, *57*, 1742.
- [12] Y. Fuchs, O. Soppera, K. Haupt, *Anal. Chim. Acta* **2011**, *717*, 7.
- [13] X. B. Hu, Q. An, G. T. Li, S. Y. Tao, B. Liu, *Angew. Chem. Int. Ed.* **2006**, *45*, 8145.
- [14] a) M. E. Byrne, K. Park, N. A. Peppas, *Adv. Drug Delivery Rev.* **2002**, *54*, 149; b) A. Mateescu, Y. Wang, J. Dostalek, U. Jonas, *Membranes* **2012**, *2*, 40.
- [15] M. Riskin, R. Tel-Vered, O. Lioubashevski, I. Willner, *J. Am. Chem. Soc.* **2009**, *131*, 7368.
- [16] D. Vaihinger, K. Landfester, I. Krauter, H. Brunner, G. E. M. Tovar, *Macromol. Chem. Phys.* **2002**, *203*, 1965.
- [17] A. Poma, A. Guerreiro, M. J. Whitcombe, E. V. Piletska, A. P. F. Turner, S. A. Piletsky, *Adv. Funct. Mater.* **2013**, *23*, 2821.
- [18] A. R. Guerreiro, I. Chianella, E. Piletska, M. J. Whitcombe, S. A. Piletsky, *Biosens. Bioelectron.* **2009**, *24*, 2740.
- [19] I. Chianella, A. Guerreiro, E. Moczko, J. S. Caygill, E. V. Piletska, I. M. P. De Vargas Sansalvador, M. J. Whitcombe, S. A. Piletsky, *Anal. Chem.* **2013**, *85*, 8462.
- [20] Y. Taguchi, E. Takano, T. Takeuchi, *Langmuir* **2012**, *28*, 7083.
- [21] Y. Wang, C. J. Huang, U. Jonas, J. Dostalek, W. Knoll, *Biosens. Bioelectron.* **2010**, *25*, 1663.
- [22] Q. Zhang, Y. Wang, A. Mateescu, U. Jonas, T. Wei, J. Dostalek, *Talanta* **2013**, *104*, 149.
- [23] C. R. van den Brom, I. Anac, R. F. Roskamp, M. Retsch, U. Jonas, B. Menges, J. A. Preece, *J. Mater. Chem.* **2010**, *20*, 4827.
- [24] N. W. Ashcroft, N. D. Mermin, *Solid State Physics*, HRW International Editions, **1976**.
- [25] M. Lehmann, M. Dettling, H. Brunner, G. E. M. Tovar, *J. Chromatogr. B* **2004**, *808*, 43.
- [26] A. Weber, M. Dettling, H. Brunner, G. Tovar, *Macromol. Rapid Commun.* **2002**, *23*, 824.
- [27] M. J. N. Junk, U. Jonas, D. Hinderberger, *Small* **2008**, *4*, 1485.
- [28] R. Slavik, J. Homola, *Sens. Actuators, B* **2007**, *123*, 10.